X-ray-absorption spectroscopy beyond the natural width measured in partial Auger yield mode

Yasen Velkov,[1,*] Yasumasa Hikosaka,[2] Eiji Shigemasa,[2] Tatsuo Kaneyasu,[2] Yusuke Tamenori,[3] Ji-Cai Liu,[1] and Faris Gel'mukhanov[1]

[1]*Department of Theoretical Chemistry, Roslagstullsbacken 15, Royal Institute of Technology, S-106 91 Stockholm, Sweden*

[2]*UVSOR Facility, Institute for Molecular Science, Okazaki 444-8585, Japan*

[3]*Japan Synchrotron Radiation Research Institute, Sayo 679-5198, Japan*

(Received 11 August 2008; revised manuscript received 1 December 2008; published 10 February 2009)

We report both experimental and theoretical studies on x-ray absorption measured using partial Auger yields of gas phase nitrogen, carbon monoxide, and oxygen molecules near the N $1s \rightarrow \pi^*$, O $1s \rightarrow \pi^*$, and O $1s \rightarrow \pi^*$ regions, respectively. The main tool of our study is a two-dimensional map in which resonant Auger yields are plotted as a function of photon and kinetic energy. The partial yields of the three molecules are analyzed in detail by extracting profiles along various directions in the map. Narrowing of the absorption resonances is observed along the direction of constant kinetic energy. It is shown that such profiles are similar to the conventional x-ray-absorption spectrum for a broad class of molecules whose potential energy surfaces of the final and core-excited states are almost parallel. However, substantial differences with the conventional x-ray-absorption profiles are observed in the general case of nonparallel surfaces due to the lifetime vibrational interference. Here, we suggest a systematic way to eliminate the lifetime vibrational interference.

DOI: 10.1103/PhysRevA.79.022508 PACS number(s): 33.20.Rm, 33.80.Eh, 34.10.+x

I. INTRODUCTION

X-ray-absorption spectroscopy (XAS) is one of the most powerful techniques for investigating composition and electronic structure of matter. This spectroscopy can provide direct information about the chemical nature and surroundings of the specific atoms constituting the probed molecular species. Consequently, XAS has been successfully used in various fields of science, such as physics, chemistry, biology, and geology [1]. Unfortunately, the spectra obtained by XAS are often extremely smeared out due inherently to the large lifetime broadenings of the core-excited states. In this respect, some achievements of superhigh resolution beyond the lifetime broadenings of core-excited states have attracted special attention. The method that has been believed to produce XAS-like spectra with superhigh resolution is the measurement of absorption profiles in the resonant x-ray Raman scattering (RXRS) or resonant Auger scattering (RAS) modes [2,3]. One might intuitively expect that these Raman scattering cross sections as a function of photon energy eventually agree with the conventional XAS profiles, because the flux of x rays and Auger electrons is caused by x-ray absorption. Moreover, a fundamental characteristic of RXRS and RAS is that their spectral resolution is not affected by the lifetime broadenings of the core-excited states [4,5] and thus supernarrow peaks can be observed on the scattering spectra [6]. Indeed, narrowing of x-ray-absorption resonances was experimentally evidenced in the scans of these scattering processes within narrow observation windows [7,8]. In other words, this spectroscopy is based on the measurement of XAS using high-resolution partial fluorescence or Auger yields (HRPY). It is worth noting that other terminologies are also used in the literature: lifetime broadening removed XAS [9], high-energy-resolution fluorescence detection absorptionlike spectra [10], fluorescence-selecting XANES [11], lifetime-broadening-suppressed selective XAFS [12], etc. Following the articles [8,13], we call this spectroscopy HRPY-XAS. Due to the importance of XAS with superhigh resolution, HRPY-XAS is a rather popular technique in x-ray spectroscopy [7–14].

It was recognized a while ago [8,15] that the HRPY-XAS and conventional XAS profiles can be very different in the general case. Furthermore, in a preceding Letter [16] we demonstrated that the supernarrow x-ray-absorption profiles obtained in the RAS mode in CO for the formation of the $A\ ^2\Pi$ final state give wrong resonance positions owing to the lifetime vibrational interference (LVI) [5,17] between core-excited vibrational levels. In the current paper, we present a more general and detailed analysis of absorption profiles in the RAS mode by extending the investigation to other molecules. The spectral pattern in the two-dimensional (2D) maps, depicting the partial Auger yields in the plane of photon and kinetic energy, is the main object of our investigation. We show that the spectral pattern is sensitive to the shapes and the relative positions of the potential energy curves of the core-excited and final states participating in the RAS processes. While various XAS profiles in the RAS mode can be extracted along different directions in the 2D maps [18], we put special emphasis on the paths along directions of constant binding energy E_B and constant kinetic energy. Narrowing of the x-ray-absorption peaks is obtained in the latter case, and an agreement with the XAS profile can be achieved for a class of molecules whose final states have quasilocalized holes and thus have potential energy curves of the final states almost parallel to the core-excited potential curves. However, for the majority of scattering final states, we face the problem that the resonance positions follow the vibrational progression of the final ionic states instead of the core-excited ones. For the purpose of overcoming this problem, we use more sophisticated paths of extraction which go

*Author to whom correspondence should be addressed. yasve@theochem.kth.se

through different hilltops in the 2D maps and cross these hilltops along the direction of constant kinetic energy. However, even with this method, we obtain incorrect positions of the resonances due to LVI. Finally, we suggest a systematic way that removes LVI completely from the 2D map and thus provides a solution to a major obstacle to HRPY-XAS. The combined experimental and theoretical results for three different molecules (N_2, CO, and O_2) allow us to gain a deep insight into the physical processes behind the HRPY-XAS technique.

We shall begin by describing the details of our experimental method as well as the experimental results in Sec. II. In Sec. III, we outline the numerical simulation technique and describe the spectroscopic parameters used in the simulations. The analysis of the XAS measurements in the RAS mode is presented in Sec. IV and is accompanied by detailed illustrations of the experimental and theoretical results. Our findings are summarized in Sec. V.

II. EXPERIMENT

The experiment was performed on the beamline 27SU [19] of SPring-8. Light from a figure-8 undulator was monochromatized by a grazing incidence monochromator. The photon bandwidth was set to around 25 meV [half-width at half-maximum (HWHM)]. The monochromatized light was introduced into a cell to which sample gases were admitted. Emitted electrons were sampled by a hemispherical electron energy analyzer (Gammadata-Scienta SES-2002) placed at a right angle with respect to the photon beam. The degree of linear polarization of the incident light was essentially 100%, and the direction of the electric vector was made parallel to the axis of the electrostatic lens of the analyzer. The kinetic energy resolution of the analyzer was set to 50 meV (HWHM). The electron transmission efficiency of this analyzer setting and the kinetic energy scale of the obtained photoelectron spectra were calibrated by measuring Ne $1s$ photoelectron peaks at different photon energies.

We have obtained RAS spectra via the N $1s \rightarrow \pi^*$ resonance into the ionic $A\ ^2\Pi_u$ state for N_2, via the O $1s \rightarrow \pi^*$ resonance into the ionic $A\ ^2\Pi$ state for CO, and via the O $1s \rightarrow \pi^*$ resonance into the ionic $X\ ^2\Pi_g$ state for O_2. Here, in every resonance range, around 100 RAS spectra were measured with small photon energy steps (15 meV). For an effective presentation of the experimental RAS spectra, they were assembled as 2D maps shown in Figs. 1(a), 2(a), and 3(a) for N_2, CO, and O_2, respectively, where intensities are plotted on individual linear scales. The horizontal axes correspond to the electron kinetic energy E, and the vertical to the photon energy ω. The 2D maps are formed by diagonal stripes, each of which corresponds to a certain vibrational level ν_f of the final ionic states. In fact, the formation of those stripes is a manifestation of the Raman law. The binding energy $E_B \equiv \omega - E$ is constant along these stripes and is equal to the energy for the direct transition $|0_0\rangle \rightarrow |\nu_f\rangle$. Here, $|0_0\rangle$ and $|\nu_f\rangle$ denote the vibrational wave funtions of the initial ground and final ionic states, respectively. These stripes consist of "hills," in the shape of ellipse, though each stripe in the 2D map for N_2 contains only one hill. One may suppose that the peak positions of the hills simply reflect the vibrational levels ν_c of the core-excited states; however, except for the N_2 case, the positions of the hilltops deviate slightly from the ν_c progressions seen on the conventional XAS spectra, which will be shown later.

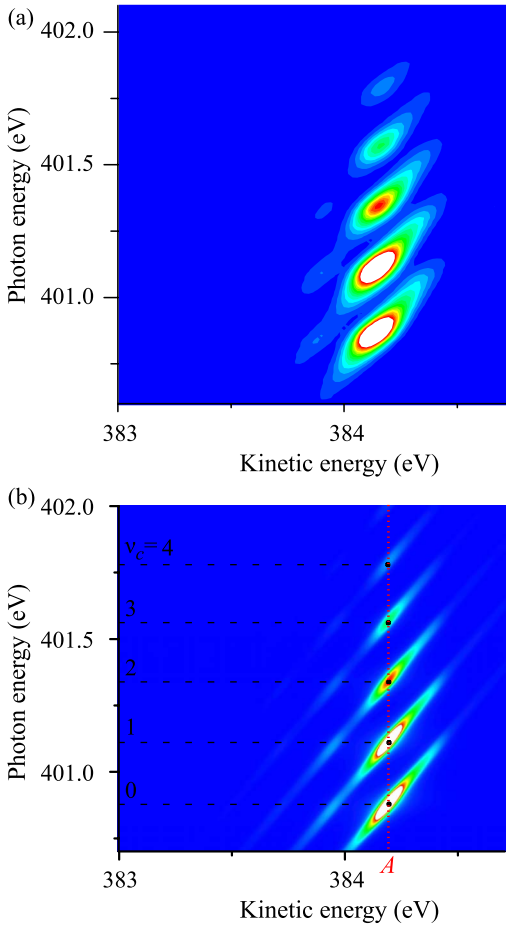

FIG. 1. (Color online) 2D map of RAS spectra of N_2 from (a) experiment and (b) theory. The horizontal dashed lines in (b) correspond to the core-excited vibrational resonances. The vertical dotted line A in (b) goes through the hilltops for $\nu_f = \nu_c$.

III. NUMERICAL SIMULATIONS

We simulated RAS for the three molecules (N_2, CO, O_2) investigated experimentally. Our simulations are based on the time-dependent (wave-packet) code [20]. The potential energy curves for the ground, core-excited, and final ionic states are assumed to be Morse functions with the parameters given in Tables I–III for N_2, CO, and O_2, respectively. In the time-dependent simulations, the lifetime broadenings (HWHM) of the final ionic states are set to $\Gamma_f = 0.01$ eV and the instrumental broadening for the present Auger energy analysis is neglected. To mimic the experimental photon profile, we set $\gamma = \gamma_1 (\ln 2)^{1/2k} = 25$ meV (HWHM) and $k=3$ for the spectral function of incident photons, $\Phi(\Omega, \gamma) = [k/\gamma_1 \Gamma(1/2k)] \exp[-(\Omega/\gamma_1)^{2k}]$. Direct photoionization is not considered because the contributions are small around the resonances studied [21–23]. The simulation output is rep-

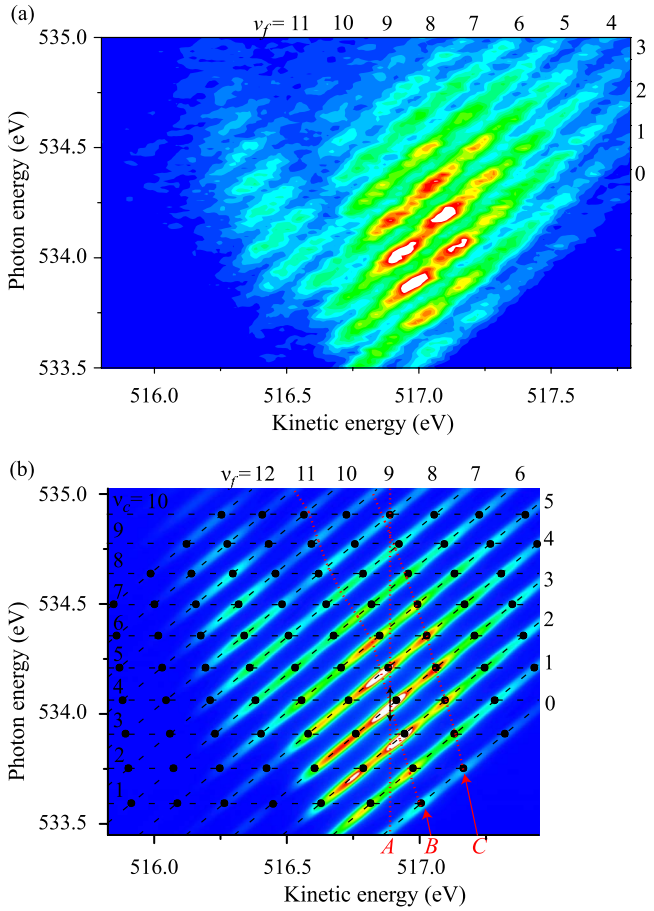

FIG. 2. (Color online) 2D map of RAS spectra of CO from (a) experiment and (b) theory. The horizontal and the diagonal dashed lines in (b) correspond to the core-excited and final-state vibrational progressions, respectively. The black dots in (b) show the peak positions of the direct term in Eqs. (5). The red dotted lines describe three paths of extracting HRPY-XAS: *A*, *B*, and *C*.

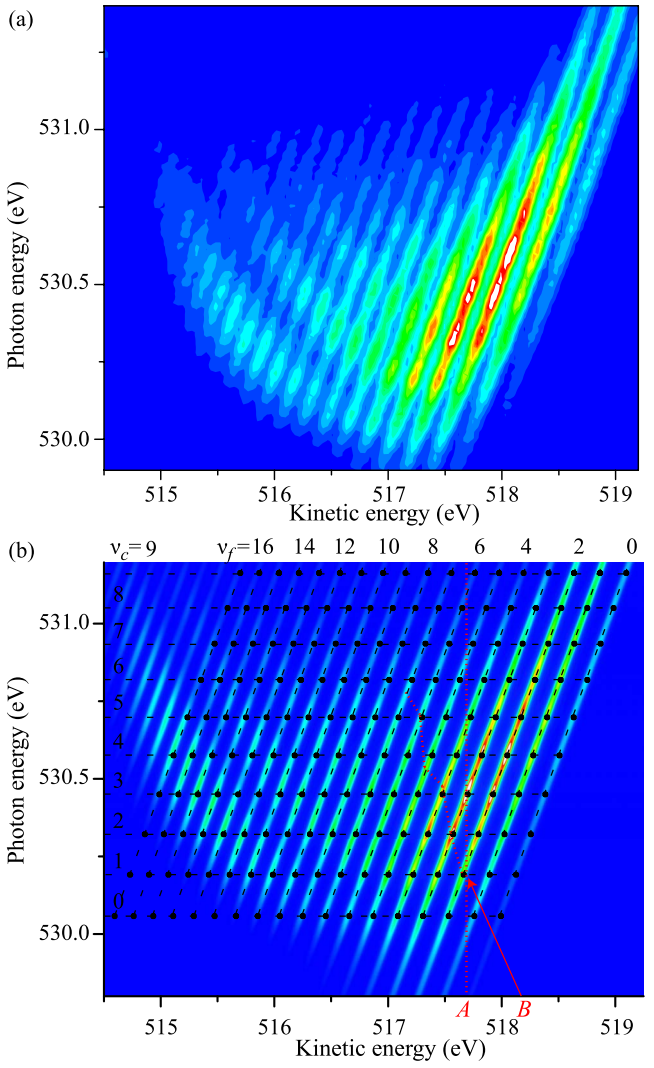

FIG. 3. (Color online) 2D map of RAS spectra of O_2 from (a) experiment and (b) theory. The horizontal and the diagonal dashed lines in (b) correspond to the core-excited and final-state vibrational progressions, respectively. The black dots in (b) show the peak positions of the direct term in Eqs. (5). The red dotted lines describe two paths of extracting HRPY-XAS: *A* and *B*.

resented as the 2D maps shown in Figs. 1(b), 2(b), and 3(b), for comparison with the experimental results.

IV. ANALYSIS OF THE EXPERIMENTAL AND THEORETICAL RESULTS

When x-ray absorption is measured in the transmission mode, the attenuation of the incident x-ray beam is characterized by the cross section of x-ray absorption,

$$\sigma_{\mathrm{XAS}}(\omega) = \sum_{\nu_c} \frac{\langle \nu_c | 0_0 \rangle^2}{(\omega - \omega_{\nu_c 0_0})^2 + \Gamma^2}. \quad (1)$$

Here, $|\nu_c\rangle$ is the vibrational wave function of the core-excited state, and Γ is the lifetime broadening of the core-excited state (HWHM). We denote with $\omega_{\nu_j \nu_i}$ the resonant energy of the vibronic transition $|\nu_i\rangle \rightarrow |\nu_j\rangle$, and $\omega_{\nu_j \nu_i} = E^e_{ji} + (\epsilon_{\nu_j} - \epsilon_{\nu_i})$. The first term E^e_{ji} on the right-hand side is the energy difference between the potential minima of the electronic states *i* and *j*, and the second term $\epsilon_{\nu_j} - \epsilon_{\nu_i}$ is the difference of the vibrational energies in the electronic states. We omit the constant prefactor including the electronic transition matrix element from both XAS and RAS cross-section expressions, because we are concerned only with the relative shape of the x-ray spectra.

In fact, x-ray absorption can be measured in various modes [1]. For example, the collection of the Auger electrons in a wide kinetic energy range gives a spectrum that strongly

TABLE I. Spectroscopic constants used for the calculation of the Morse potential curves of the N_2 molecule.

	ω_e (cm^{-1})	$\omega_e x_e$ (cm^{-1})	R_e (Å)	T_e (eV)	Γ (eV)
$\|0\rangle$ $(X\ ^1\Sigma_g^+)^a$	2358.57	14.324	1.09768	0	
$\|c\rangle$ $(^1\Pi_u)^b$	1904.1	17.235	1.1645	400.9083	0.0575
$\|f\rangle$ $(A^2\Pi_u)^a$	1903.7	15.02	1.1749	16.7173	

[a]From Ref. [31].
[b]From Ref. [22].

TABLE II. Spectroscopic constants used for the calculation of the Morse potential curves of the CO molecule. Data taken from [21].

	ω_e (cm^{-1})	$\omega_e x_e$ (cm^{-1})	R_e (Å)	T_e (eV)	Γ (eV)
$\|0\rangle$ ($X\,^1\Sigma^+$)	2169.84	13.292	1.1283	0	
$\|c\rangle$ ($^1\Pi$)	1346.98	12.905	1.288	533.4692	0.078
$\|f\rangle$ ($A\,^2\Pi$)	1562.09	13.534	1.244	16.6227	

resembles the XAS profile (1) with resonance widths equal to the lifetime broadening of the core-excited state [24]. For obtaining resolution better than the natural lifetime broadening, Tulkki and Åberg [2], and later Drube *et al.* [3], suggested a technique of x-ray-absorption measurement using the RXRS or RAS modes. More precisely, the suggested instruction was to scan over the photon energy while keeping the kinetic energy fixed at the maximum of the Raman scattering profile; this produces absorption spectra based on the partial final-state yields or HRPY-XAS. In the present study, however, we do not restrict our investigation to the HRPY-XAS technique only, but instead we use also other approaches giving insight into the dependence of the RAS profile on the photon energy.

The spectral properties of the RAS cross section [5]

$$\sigma_{\mathrm{RAS}}(\omega,E)=\sum_{\nu_f}|F_{\nu_f}|^2\Phi(\omega-E-\omega_{\nu_f 0_0},\gamma) \tag{2}$$

are given by the spectral function $\Phi(\Omega,\gamma)$ and the Kramers-Heisenberg scattering amplitude

$$F_{\nu_f}=\sum_{\nu_c=0}^{\infty}F_{\nu_f\nu_c},\quad F_{\nu_f\nu_c}=\frac{\langle\nu_f|\nu_c\rangle\langle\nu_c|0_0\rangle}{E-\omega_{\nu_c\nu_f}+\imath\Gamma}, \tag{3}$$

which is a coherent sum over the paths through different ν_c. As mentioned above, we neglect the rather weak direct photoionization: The amplitude of the direct channel ($\propto\langle\nu_f|0_0\rangle$) is not included in the expression for the RAS amplitude in Eqs. (3). One might expect intuitively that the RAS cross section as a function of ω eventually agrees with the conventional XAS profile, because the flux of Auger electrons is caused by x-ray absorption. However, on closer inspection of the equations above, one realizes that the RAS profile can deviate from the conventional XAS profile due to the Franck-Condon (FC) amplitude $\langle\nu_f|\nu_c\rangle$, the interference of the intermediate core-excited states in the terms $F^*_{\nu_f\nu_c'}F_{\nu_f\nu_c}$, and the spectral function $\Phi(\Omega,\gamma)$.

TABLE III. Spectroscopic constants used for the calculation of the Morse potential curves of the O_2 molecule.

	ω_e (cm^{-1})	$\omega_e x_e$ (cm^{-1})	R_e (Å)	T_e (eV)	Γ (eV)
$\|0\rangle$ ($X\,^3\Sigma_g^-$)[a]	1580.19	11.98	1.2074	0	
$\|c\rangle$ ($^3\Pi_u$)[b]	1097.18	10.75	1.3540	530.095[c]	0.07475[d]
$\|f\rangle$ ($X\,^2\Pi_g$)[a]	1904.7	16.259	1.1162	12.0612[e]	

[a]From Ref. [31].
[b]From Ref. [23].
[c]Fitted to the experimental data.
[d]From Ref. [28].
[e]From Ref. [32].

A. Patterns on the 2D map of Auger yields

It is convenient to analyze the spectral patterns seen in Figs. 1–3 by separating the RAS cross section (2) into direct (not to be confused with the direct photoionization) and interference contributions,

$$\sigma_{\mathrm{RAS}}(\omega,E)=\sigma_{\mathrm{dir}}(\omega,E)+\sigma_{\mathrm{int}}(\omega,E). \tag{4}$$

According to Eqs. (3), these contributions have the following forms:

$$\sigma_{\mathrm{dir}}(\omega,E)=\sum_{\nu_f,\nu_c}\frac{\langle\nu_f|\nu_c\rangle^2\langle\nu_c|0_0\rangle^2\Phi(E_B-\omega_{\nu_f 0_0},\gamma)}{(E-\omega_{\nu_c\nu_f})^2+\Gamma^2},$$

$$\sigma_{\mathrm{int}}(\omega,E)=\sum_{\nu_f}\sum_{\nu_c'\neq\nu_c}F^*_{\nu_f\nu_c'}F_{\nu_f\nu_c}\Phi(E_B-\omega_{\nu_f 0_0},\gamma). \tag{5}$$

The direct term $\sigma_{\mathrm{dir}}(\omega,E)$ is a product of the Lorentzian and the spectral functions, both of which are dependent on two variables. That is, the direct term constructs "hills" having elliptical shapes in the 2D plane of (ω,E), similar to those observed on the 2D maps in Figs. 1–3. The location of the direct-term hills with respect to ω matches exactly with the resonances of the conventional XAS spectrum. The peak positions of the direct-term hills have coordinates at $(\omega,E)=(\omega_{\nu_c 0_0},\omega_{\nu_c\nu_f})$, which are marked with black dots in Figs. 1(b), 2(b), and 3(b). One can see that the peak positions of the direct-term hills do not coincide strictly with those of the real hills (except for N_2), as will be discussed shortly.

The easiest way to envisage the resolution of the profiles of the 2D map is to look at the direct term in Eqs. (5). The cross sections of the direct-term hills along the major elliptical axes ($E_B=\omega_{\nu_f 0_0}=$const) passing through the peaks of the hills,

$$\sigma_{\mathrm{dir}}(\omega,E)=\Phi(0,\gamma)\sum_{\nu_c}\frac{\langle\nu_f|\nu_c\rangle^2\langle\nu_c|0_0\rangle^2}{(\omega-\omega_{\nu_c 0_0})^2+\Gamma^2}, \tag{6}$$

would not display a better resolution than Γ, because the spectral function is just a constant factor in this equation. This is in agreement with the patterns along the stripes observed on the 2D maps. On the other hand, the cut of each hill along the ω axis ($E=\omega_{\nu_c 0_0}-\omega_{\nu_f 0_0}=$const),

$$\sigma_{\mathrm{dir}}(\omega,E)=\frac{1}{\Gamma^2}\langle\nu_f|\nu_c\rangle^2\langle\nu_c|0_0\rangle^2\Phi(\omega-\omega_{\nu_c 0_0},\gamma), \tag{7}$$

provides a supernarrow resonance whose width is equal to the spectral-function width γ. In practice, each hill on the individual diagonal stripes on the 2D maps shows a narrower width along the ω axes. The idea of HRPY-XAS relies on this fact.

We pause here to comment on the distributions of the hilltop positions on the 2D maps. To understand the distribution, we draw a scheme of the peak positions of the direct-

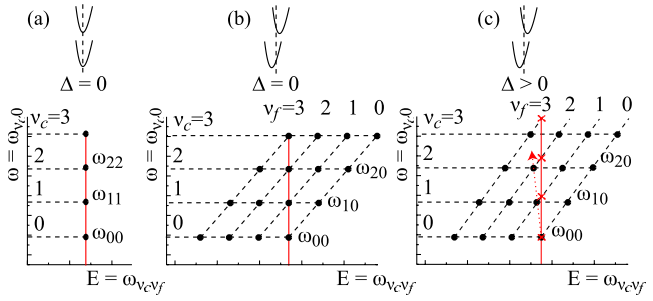

FIG. 4. (Color online) Distribution scheme of the direct term hilltops in Eqs. (5) for three cases of core-excited and final states: (a) strictly parallel potential curves; (b) shifted potential curves with the same vibrational frequency; (c) shifted potential curves with different vibrational frequencies. The vertical solid lines correspond to E=const. The red crosses in (c) mark the crossing points between the vertical lines and the diagonal E_B-fixed lines. The dotted arrow shows an alternative extraction path.

term hills (Fig. 4) within the harmonic approximation. Thus, the peaks have coordinates $(\omega_{\nu_c 0_0}, \omega_{\nu_c \nu_f})$ wherein $\omega_{\nu_c \nu_f}$ is restricted to

$$\omega_{\nu_c \nu_f} = (\nu_c - \nu_f)\omega_c - \left(\nu_f + \tfrac{1}{2}\right)\Delta + E^e_{cf}. \tag{8}$$

Here, $\Delta = \omega_f - \omega_c$ is the difference between the vibrational frequencies ω_f and ω_c of the final and the core-excited potential energy curves, respectively. The hilltop positions for three qualitatively different relations between the core-excited and final potential energy curves are depicted in Fig. 4. When the potential energy curves are perfectly parallel to each other, only decay transitions without a change of the vibrational quantum number (i.e., $\nu_f = \nu_c$) are allowed (see Sec. IV B for more details). In this case, the hilltops are aligned on a single vertical line with $E = \omega_{\nu_c \nu_f}$=const [see Fig. 4(a)]; this is observed on the 2D maps of N_2 (Fig. 1). When the potential energy curves are shifted with respect to each other, decay transitions with a change of the vibrational quantum number are also allowed (i.e., $\nu_f \neq \nu_c$). Therefore, the hilltops are distributed in the (ω, E) plane and form a grid of points [see Figs. 4(b) and 4(c)]. The alignment of the hilltops depends on Δ: When $\Delta = 0$, the hilltops are aligned along vertical lines with E=const and form a square grid [Fig. 4(b)], as is immediately understood from Eq. (8). On the other hand, when $\Delta \neq 0$ the hilltops are aligned along tilted lines with $E \neq$ const and form a rhomboidal grid [Fig. 4(c)]; this is the case with the 2D maps of CO and O_2 (Figs. 2 and 3). The angle of tilting depends on the magnitude and the sign of Δ.

B. Binding-energy fixed profiles of N_2, CO, and O_2

It was noticed in the previous section that HRPY-XAS can be achieved by extracting partial RAS yields at E fixed onto a given peak $(E = \omega_{\nu_c \nu_f})$ of the direct-term hills. Unfortunately, it was also observed that the real hilltops on the 2D maps generally differ from the direct-term hilltops. In this section, we analyze the origin of the differences. Owing to the inherited similarities between Eqs. (1) and (6), it is convenient to analyze those differences by extracting absorption profiles in the RAS mode at E_B=const. As mentioned above, the spectral function in Eq. (6) is just a constant and can be neglected. A comparison between Eqs. (1) and (5) shows that the difference in the spectral shape is determined by two factors: the FC factors $\langle \nu_f | \nu_c \rangle^2$ and the interference term in Eqs. (5). In practice, the magnitudes of $\langle \nu_f | \nu_c \rangle$ and the interference between the intermediate states are determined essentially by the parameters of the core-excited and final potential energy curves. It is therefore instructive to organize the discussion of the E_B-fixed profiles according to the interrelations between the core-excited and final potential energy curves.

1. Spectral shape of the E_B-fixed profiles

We start with the special case where the core-excited and final potential energy curves are parallel. In this situation, the FC factors of the decay transition are drastically simplified because

$$\langle \nu_f | \nu_c \rangle = \delta_{\nu_f \nu_c}. \tag{9}$$

The RAS amplitude of Eq. (3) depends now only on the FC factor of the direct transition from the ground to the final state,

$$F_{\nu_f} = \frac{\langle \nu_f | 0_0 \rangle}{E - E^e_{cf} + \imath\Gamma}, \tag{10}$$

and the resonant frequency of the decay transition E^e_{cf} does not depend on the vibrational states, because $\epsilon^f_\nu = \epsilon^c_\nu$. This leads to the so-called collapse effect [5,25,26]. Such a situation can be observed in a number of molecules [22,25,27], including RAS in N_2, which we investigate here (see Table I). The E_B-fixed profiles of N_2 for several ν_f are shown in Fig. 5, where the experimental spectra are extracted from the 2D map by applying least-squares fitting with sums of Gaussian-function peaks to the ν_f distribution at each photon energy. One observes just a single resonance for each of the selected $E_B = \nu_f$, because each $|\nu_f\rangle$ overlaps almost strictly with only one $|\nu_c\rangle$ having the same vibrational quantum number. There are no shifts of the resonance positions relative to the XAS spectrum, as predicted by Eqs. (9) and (10).

Next we turn to the more common case in which the core-excited and final potential energy curves are displaced and the E_B-fixed profiles obey the general equations (5) and (6). The first example is RAS in CO where the displacement between the core-excited and the final potential energy curves is relatively small (see Table II). Figure 6 shows the E_B-fixed profiles of CO tuned to several ν_f. Despite the small shift between the potential energy curves, both theory and experiment display drastic differences between the shapes of the E_B-fixed and the XAS resonances. In contrast to N_2, the E_B-fixed bands have broad shapes due to multiple overlaps of each $|\nu_f\rangle$ with several $|\nu_c\rangle$. The peaks on the E_B-fixed bands evidently show shifts with respect to the XAS spectrum. The main reason for the peak shifts is the LVI term $\sigma_{\text{int}}(\omega, E)$ in Eqs. (5). In order to make this point very clear, we present in Fig. 7 the contributions from the direct and the interference terms to the formation of the ν_f=2 band. The interference

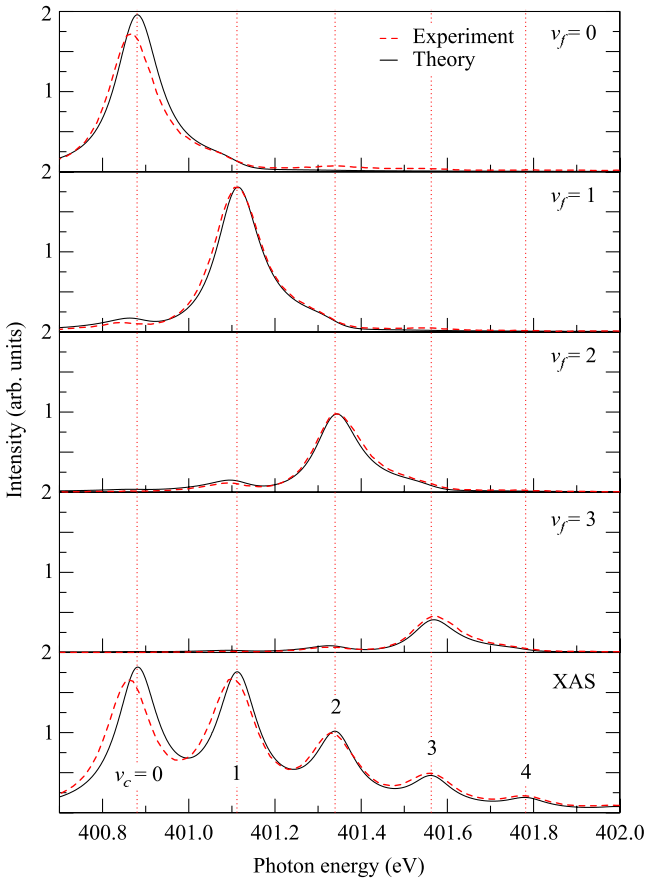

FIG. 5. (Color online) E_B-fixed spectra of N_2 tuned to ν_f=0–3 (extracted from Fig. 1) and conventional XAS spectra. The vertical dotted lines indicate the XAS resonances.

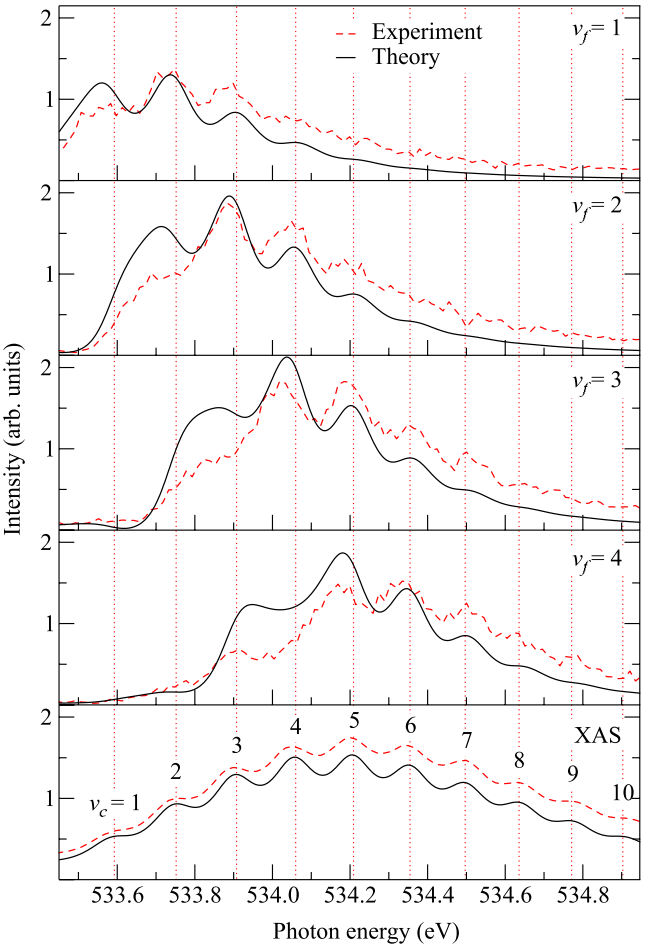

FIG. 6. (Color online) E_B-fixed spectra of CO tuned to ν_f=1–4 (extracted from Fig. 2) and conventional XAS spectra. The vertical dotted lines indicate the XAS resonances.

here has such a crucial effect that it erases some of the direct-term peaks and creates new peaks at completely different positions from the real XAS resonances. The second example of displaced potential energy curves that we examine is RAS in O_2. The displacement between the core-excited and the final potential energy curves is comparatively large here (see Table III). As a consequence, each $|\nu_f\rangle$ overlaps with a great number of $|\nu_c\rangle$. The E_B-fixed profiles for several ν_f of O_2 are plotted in Fig. 8, where one can observe broad shapes for each profile. It is worth mentioning that the RAS profiles are quite sensitive to the quality of the core-excited potential energy curves. While the agreement between the theoretical and experimental profiles is fairly good in all the studied cases with the parameters used currently, the parameters taken from [28] result in relatively poor agreements.

2. *Center of gravity of the binding-energy-fixed profiles*

The dispersion law of the center of gravity of the E_B-fixed profiles for different ν_f deserves a special comment. The dispersion was investigated previously in a different context in [29]. In order to understand the dispersion more closely, we present in Fig. 9 a scheme of the potential energy curves of the studied RAS in N_2, CO, and O_2. In the case of N_2, the potential energy curves of the core-excited and final states are almost parallel and the vibrational wave functions are orthonormal. Therefore, the decay transitions from each ν_c form only one peak ν_f with the same vibrational number. Hence, the E_B-fixed band moves to higher photon energy

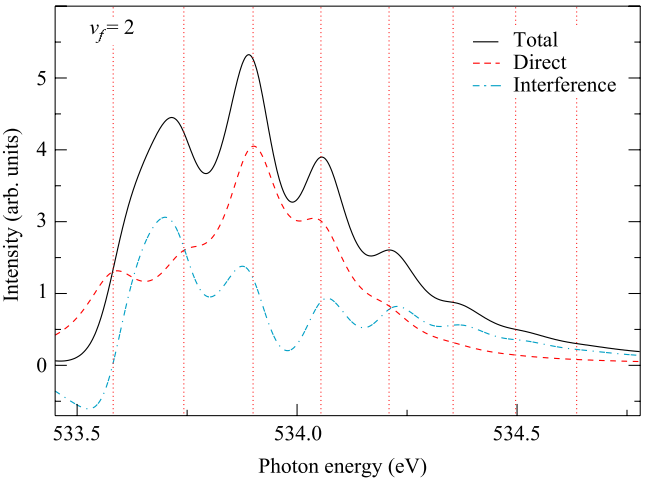

FIG. 7. (Color online) Direct and interference contributions to the theoretical E_B-fixed spectrum of CO tuned to ν_f=2. The vertical dotted lines indicate the XAS resonances.

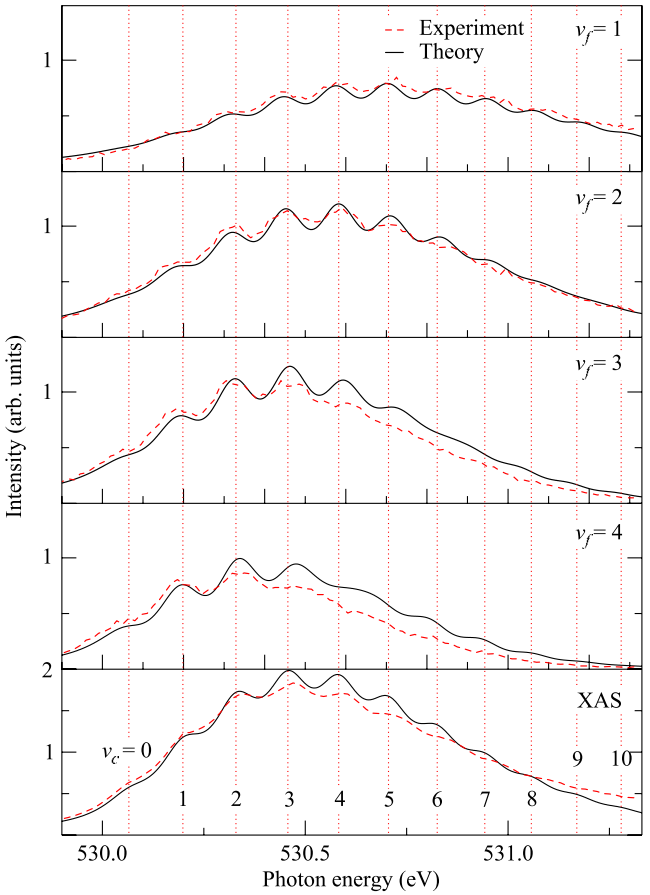

FIG. 8. (Color online) E_B-fixed spectra of O_2 tuned to $\nu_f = 1-4$ (extracted from Fig. 3) and conventional XAS spectra. The vertical dotted lines indicate the XAS resonances.

when higher binding energy partial yields are selected, as seen in Fig. 5. In the case of CO, though the forms of the core-excited and final potential energy curves are fairly similar, the equilibrium positions are slightly displaced (see Fig. 9). Consequently, each $|\nu_f\rangle$ overlaps with many $|\nu_c\rangle$ in the regions of both left and right classical turning points, resulting in a broad E_B-fixed band. However, higher ν_f still selects predominantly higher ν_c and the center of gravity moves to higher photon energy (see Fig. 6), similarly to N_2.

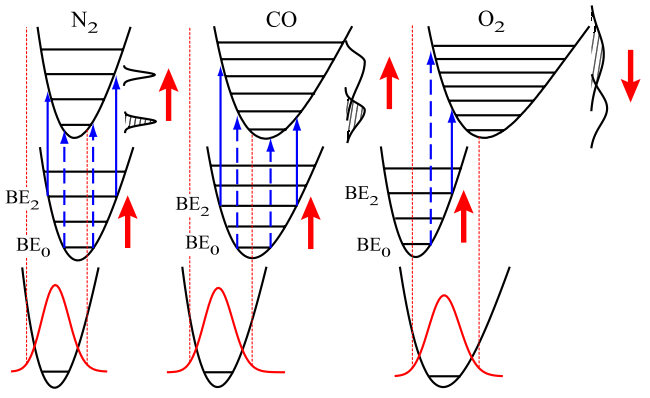

FIG. 9. (Color online) Scheme of the potential energy curves of the neutral ground, the core-excited, and the final ionic states of N_2, CO, and O_2. The red arrows indicate the dispersion of the center of gravity of the E_B-fixed profiles for increasing final-state vibrational numbers.

Lastly, in the case of O_2, the potential energy curves of the core-excited and final ionic states are rather dissimilar and displaced, as depicted in Fig. 9. In fact, the left classical turning points of $|\nu_f\rangle$ are situated outside the FC region of the ground-state wave function and are not relevant to the scattering process. The region of right turning points of $|\nu_f\rangle$ overlaps with that of left turning points of $|\nu_c\rangle$, and, therefore, higher ν_f selects lower ν_c. This causes the peculiar dispersion of the center of gravity of the E_B-fixed bands seen in Fig. 8, which is opposite to the previous two cases. Although the overlap here occurs at only one side, the observed E_B-fixed profiles are much broader than the profiles in the CO case. This is due to the fact that the core-excited state of O_2 has a denser vibrational progression and more delocalized vibrational wave functions. Thus, each $|\nu_f\rangle$ overlaps with a greater number of $|\nu_c\rangle$.

C. Profiles with superhigh resolution

The analysis performed in the previous sections shows that the resonance positions in the E_B-fixed spectra deviate, mainly due to LVI, from those in the conventional XAS. In this section, we demonstrate why LVI leads to practical limitations of HRPY-XAS, which, in the general case, are difficult to avoid by the classic technique suggested by Tulkki and Åberg [2].

1. HRPY-XAS for E fixed at the global maximum of the 2D map

A HRPY-XAS profile with resolution beyond the lifetime broadening of the core-excited state can be achieved when it is extracted from the 2D map along constant kinetic energy (see Sec. IV A). We show here that this method works correctly only in the special case of parallel potential energy curves of the core-excited and final states. In all other cases, this technique produces imprecise positioning of the HRPY-XAS resonances in comparison with the conventional XAS profile.

HRPY-XAS for similar core-excited and final potential energy curves. Let us start with the N_2 case, in which the potential energy curves of the core-excited and final states are parallel. It is natural to fix the constant kinetic energy at the global maxima of the 2D maps (Fig. 1). The extracted HRPY-XAS spectra are shown in Fig. 10. In practice, while the theoretical spectrum is extracted along $E = E_{\max} = 384.191$ eV (the red line indicated in Fig. 1), the experimental curve results from the integration of the yields in a narrow E range of 384.10–384.14 eV. One can see from Fig. 10 that this method works well: The HRPY-XAS profiles thus obtained follow closely the ν_c progression seen in the conventional XAS spectrum, which is in agreement with a previous study [8]. The resonances in the HRPY-XAS spectra are much narrower than those in the conventional XAS spectrum, because the HRPY-XAS profile of Eq. (4) is simply proportional to the narrow spectral function $\Phi(\omega - E_{\max}$

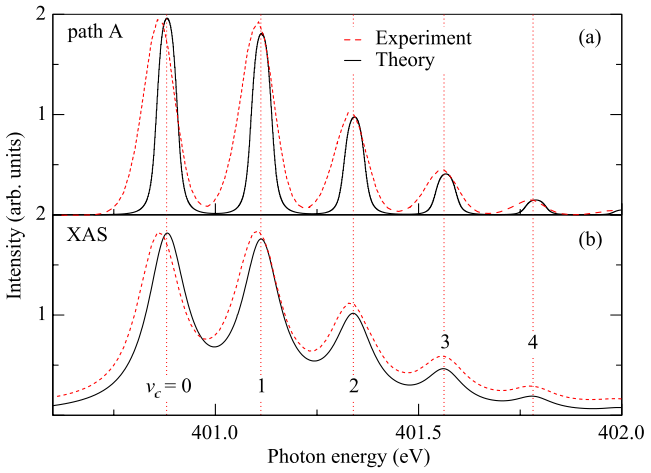

FIG. 10. (Color online) (a) HRPY-XAS spectra of N_2 along path *A* [Fig. 1(b)], $E=E_{\max}=384.191$ eV for theory and $E=384.10-384.14$ eV for experiment. (b) Conventional XAS spectra of N_2. The vertical lines indicate the XAS resonances.

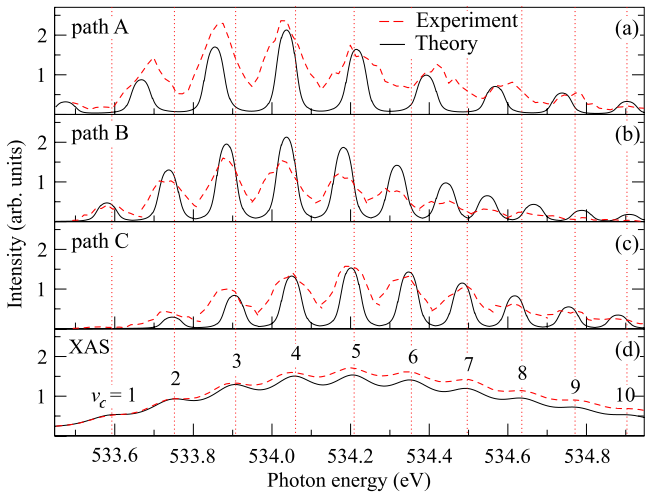

FIG. 11. (Color online) (a) HRPY-XAS spectra of CO along path *A* [Fig. 2(b)], $E=E_{\max}=516.89$ eV for theory and $E=516.93-516.97$ eV for experiment. (b) HRPY-XAS spectra of CO following path *B* [Fig. 2(b)]. (c) XAS spectra of CO following path *C* [Fig. 2(b)]. (d) Conventional XAS spectra of CO. The vertical dotted lines indicate the XAS resonances.

$-\omega_{\nu_f 0_0}, \gamma$). Slight disagreements may be seen in the positions of the resonances at higher vibrational numbers because the core-excited and final potential energy curves are not strictly parallel. The main reasons why the concept of the HRPY-XAS spectrum beyond the lifetime broadening of core-excited states is practically valid in this case are that the vibrational frequencies of the core-excited and final states are almost the same and LVI is absent.

The results for N_2 demonstrate that HRPY-XAS can be achieved in the case of molecules with almost parallel potential energy curves of the core-excited and final states. Our survey indicates that this situation is actually not as rare as one might expect. It is likely that this situation may appear often in heteronuclear molecules: Parallelism in the potential energy curves may occur between a core-excited and an ionic state whose holes have the same atomic origin. This can be observed, for example, for the $C\ 1s \rightarrow \pi^*$ core-excited state and the ionic $B\ ^2\Sigma^+$ state in CO [25]. Other related examples are the RAS (and RXRS) from a *K*-hole state to an *L*-hole state in molecules having a heavier element (P, S, Cl, etc.) [27]. Here the described technique can provide dramatically improved HRPY-XAS resolution against the extremely wide *K*-hole natural width. However, one should keep in mind that, because of the molecular field and the exchange splittings, it is not easy to utilize a final state with an *L* hole [30] for the described purpose. Nevertheless, the parallelism in the potential energy curves of the core-excited and final states can be easily judged experimentally, because the parallel case shows the peculiar 2D spectral pattern seen in Fig. 1.

HRPY-XAS for different core-excited and final potential energy curves. The idea to fix the kinetic energy at the global maximum of the 2D map, unfortunately, fails in the CO and O_2 cases. Here the potential energy curves of the core-excited and final states have different shape and, hence, the vibrational frequencies of these states are different. Figure 11(a) shows the HRPY-XAS spectra of CO extracted from the 2D maps along the direction of constant *E*. The theoretical spectrum corresponds to the cut going through the global maximum of the 2D map at $E=E_{\max}=516.89$ eV, which is indicated in Fig. 2(b) as path *A*, while the experimental one results from the integration of the yields in the range of $E=516.93-516.97$ eV. Both the experimental and theoretical spectra show sharp peaks whose widths are apparently narrower than the natural width of the core-excited state. However, the peak positions of the resonances do not coincide with the ν_c progression seen on the conventional XAS spectrum. A similar disagreement between the peak positions of the corresponding HRPY-XAS and conventional XAS profiles is observed in O_2. The HRPY-XAS spectra of O_2, extracted at $E=E_{\max}=517.68$ eV for theory and in the range $E=517.70-517.74$ eV for experiment, are shown in Fig. 12(a).

It is worth investigating in more detail the positioning of the peaks extracted at fixed *E*. If we fix the kinetic energy at given $E=\omega_{\nu_c^0 \nu_f^0}$, in the harmonic approximation, we obtain a vibrational progression with resonances at

$$\omega = E + \omega_{\nu_f 0_0} = (\nu_f - \nu_f^0)(\omega_c + \Delta) + \mathcal{E},$$

$$\mathcal{E} = E_{c0}^e + \left(\nu_c^0 + \tfrac{1}{2}\right)\omega_c - \frac{\omega_0}{2}, \tag{11}$$

where $\mathcal{E}$ collects the terms that are not dependent on the vibrational number ν_f. Apparently, this progression corresponds to the ν_c progression only when the vibrational frequencies of the core-excited and final states are the same, i.e., $\Delta=0$, otherwise the progression follows the ν_f progression. This fact is schematically illustrated in Fig. 4: The peak positions of the HRPY-XAS profile at $E=\text{const}$ (11) are produced by the crossings between the vertical lines (the red

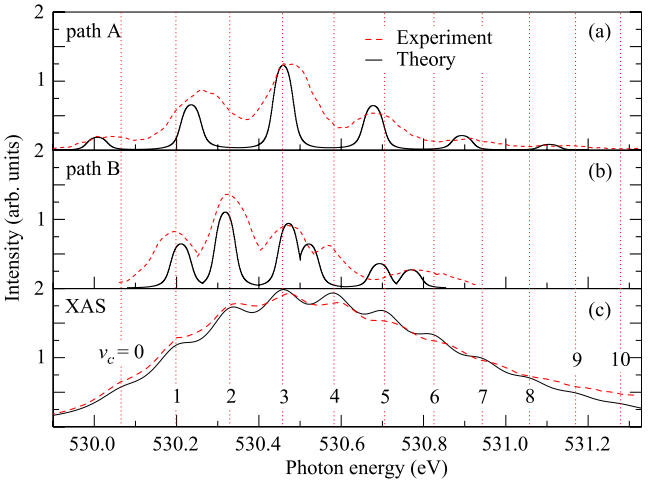

FIG. 12. (Color online) (a) HRPY-XAS spectra of O_2 along path A [Fig. 3(b)], $E=E_{max}=517.68$ eV for theory and $E=517.70-517.74$ eV for experiment. (b) HRPY-XAS spectra of O_2 following path B [Fig. 3(b)]. (c) Conventional XAS spectra of O_2. The vertical dotted lines indicate the XAS resonances.

lines in the figure) and the diagonal Raman stripes corresponding to fixed E_B. The points of crossing are shown with red crosses in Fig. 4(c). Only when $\Delta=0$ do the crossing points coincide with the conventional XAS resonances at $\omega=\omega_{\nu_c 0_0}$, represented by horizontal lines. This relation is independent of the relative shift between the core-excited and final state potential energy curves, as can be seen in Figs. 4(a) and 4(b).

2. Alternative paths for extraction of HRPY-XAS

Apparently, the HRPY-XAS spectroscopy is meaningful only if it gives the same positions of the resonances as the conventional XAS. In an effort to overcome the problem in the HRPY-XAS profile that copies the ν_f progression, instead of the vertical path through the global maximum, we adopt a more sophisticated path of extracting HRPY-XAS profiles which follows the local maxima of the 2D map. Let us recall that the direct term of Eqs. (5) is a product of the Lorentzian and the spectral functions that produces hills with tops at coordinates given by Eq. (8); the peak positions of these hills are marked by the black dots in Fig. 4. It is to be recalled also that the peak positions of the direct-term hills along the ω axis coincide exactly with the XAS resonances at $\omega=\omega_{\nu_c 0_0}$ (the horizontal lines in Fig. 4). This prompts us to change the path in the case in which $\Delta\neq 0$ in the following manner: Instead of a vertical path, we have to choose a path connecting neighboring hilltops similar to the trajectory drawn with a dashed arrow in Fig. 4(c). This trajectory is tilted from the vertical line. The angle and the direction of tilting depend on the sign and the magnitude of Δ, according to Eq. (8).

In this way of extraction, we can obtain narrow HRPY-XAS resonances by scanning over ω in the *vicinity* of each peak while keeping E fixed at the local maximum. To get the complete set of resonances, we need to tune E to each particular local maximum. However, we face here an ambiguity in the choice of path through the hilltops. That would not be a real problem only if all chosen paths produced the same HRPY-XAS profiles as the conventional XAS. To check this point we select two paths, B and C, shown in Fig. 2(b) for CO, while a single path, indicated with B in Fig. 3(b), is chosen for O_2. The HRPY-XAS spectra of superhigh resolution following these extraction paths are presented in Figs. 11(b) and 11(c) for CO and in Fig. 12(b) for O_2. Even a rough comparison between the envelopes of the HRPY-XAS profiles with the conventional XAS profiles shows large disagreement in the peak positions. In addition, one can see in Figs. 11(b) and 11(c) that the positions of the HRPY-XAS resonances, as well as the HRPY-XAS envelopes, are sensitive to the choice of paths. The deviations of the HRPY-XAS peaks result essentially from LVI (see Sec. IV B). The interference shifts manifest that XAS beyond the lifetime broadening of the core-excited states is unachievable even with the extraction method employing sophisticated paths. The lifetime broadening free regime is to be desired basically when the spacings between the core-excited levels are much smaller than Γ and the resonance maxima of the core-excited levels are hardly recognizable in the conventional XAS spectrum. Since the interference between the core-excited levels is considerably large in such cases, the resultant HRPY-XAS profiles obtained in "a lifetime broadening free regime" are profoundly different from the conventional XAS ones. Fortunately, we are able to suggest a way to eliminate LVI.

D. 2D map free from LVI

The above discussion showed that the main obstacle to the extraction of HRPY-XAS profiles is the LVI effect. However, we can describe a general procedure that removes LVI completely from the 2D map of RAS cross sections. The procedure can be applied when the 2D map consists of clearly separable ridges, as for example in Fig. 3, which is observed when $\gamma \ll \omega_f$. When the last condition is satisfied, by introducing detuning from the final-state resonance ν_f,

$$\varepsilon \equiv E_B - \omega_{\nu_f 0_0} = \text{const}, \tag{12}$$

we can write down an expression for the RAS cross section valid along all ridges,

$$\sigma_{\text{RAS}}(\omega,E) = \Phi(\varepsilon,\gamma)|F_{\nu_f}|^2, \quad F_{\nu_f} = \sum_{\nu_c=0}^{\infty} \frac{\langle \nu_f|\nu_c\rangle\langle\nu_c|0_0\rangle}{\omega-\omega_{\nu_c 0_0}-\varepsilon+\imath\Gamma}. \tag{13}$$

Let us now shift each ridge ν_f to the position of the first ridge $\nu_f=0$ and sum the intensities. The condition of completeness,

$$\sum_{\nu_f,\nu_c'} \langle 0_0|\nu_c'\rangle\langle\nu_c'|\nu_f\rangle\langle\nu_f|\nu_c\rangle\langle\nu_c|0_0\rangle = \langle 0_0|\nu_c\rangle^2, \tag{14}$$

cancels the interference term, and we finally get

$$\sigma_{\text{RAS}}(\omega,E) = \Phi(\varepsilon,\gamma)\sum_{\nu_c=0}^{\infty} \frac{\langle 0_0|\nu_c\rangle^2}{(\omega-\omega_{\nu_c 0_0}-\varepsilon)^2+\Gamma^2}. \tag{15}$$

This equation is almost identical to Eq. (1), except that the conventional XAS is multiplied by the narrow spectral func-

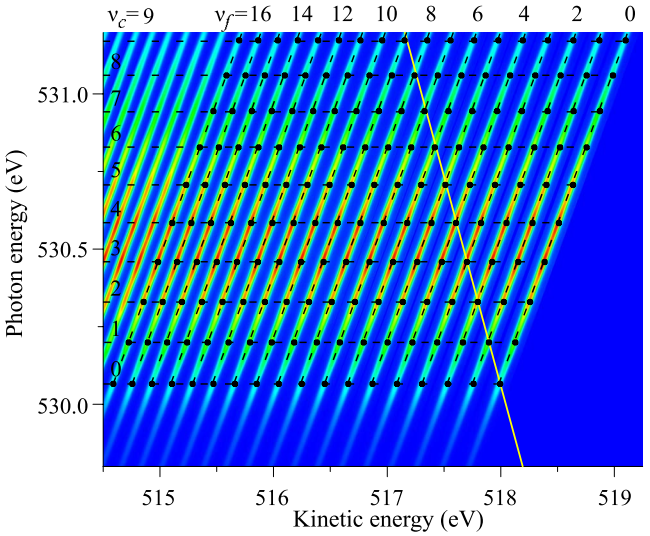

FIG. 13. (Color online) LVI-removed 2D map of O_2. All ridges have been shifted and summed for each final state ν_f. The tilted line indicates the direction of extracting HRPY-XAS.

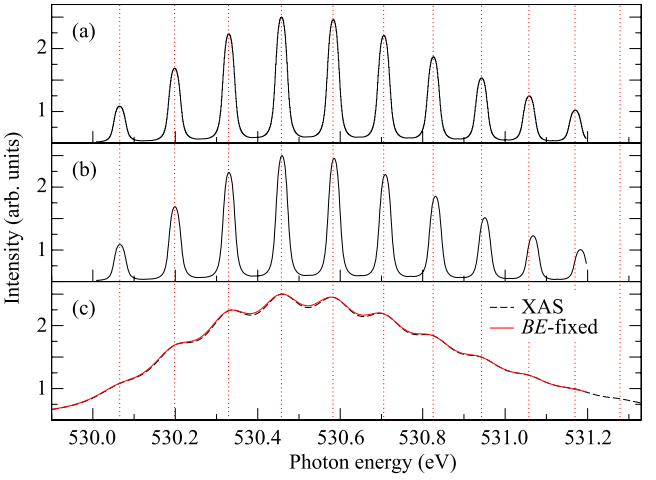

FIG. 14. (Color online) Profiles extracted from the LVI-removed 2D map (Fig. 13): (a) anharmonicity is taken into account; (b) along a straight line (harmonic approximation); (c) E_B-fixed and XAS profiles.

tion. Repeating the same procedure for all other ridges $\nu_f > 0$, we get a purified 2D map of RAS cross sections (see Fig. 13): Now the E_B-fixed profile along each ridge coincides exactly with the conventional XAS [Fig. 14(c)]. Even though we use just a limited number of final states, we obtain a good agreement with the conventional XAS. This means that the convergence is good and the condition of completeness is not broken for a limited number of terms.

Having removed LVI, we can now attempt to extract supernarrow profiles in the ways suggested in the previous section. Above, we concluded that HRPY-XAS can be extracted along a nonvertical path [see eq. (11) and Fig. 4]. Figure 14(b) shows the high-resolution profile extracted along the tilted nonvertical direction in the purified 2D map. One can see that, due to the anharmonicity, the peaks do not lie precisely on a straight line and deviations appear for higher vibrational numbers. We take into account the anharmonicity by using a path through the hilltops that deviates slighly from the straight line for higher vibrational states. Thus, when the anharmonicity is also taken into account, a high-resolution absorptionlike profile is readily obtained [Fig. 14(a)]. The last figure presents the HRPY-XAS free from any interference. However, one should keep in mind that LVI is not the only problem for the high-resolution inner-shell spectroscopy. The requirement that the hilltop positions on the 2D map must be determined in advance constitutes another major constraint [18].

V. SUMMARY

We studied both experimentally and theoretically two-dimensional RAS maps of three molecules: N_2, CO, and O_2. We analyzed in detail the shape and the distribution of the spectral patterns observed on the maps. Three different approaches were used in the extraction of high-resolution partial yield spectra from the 2D maps: at fixed binding energy, at fixed kinetic energy, and using paths through the hilltops seen on the 2D maps. Resonances with supernarrow widths were achieved in the latter two cases. However, the peak positions obtained by the extraction at fixed kinetic energy followed the vibrational progression of the final state instead of the core-excited one. The last method of extraction overcame this difficulty, but it faced another problem caused by the lifetime vibrational interference. Indeed, it was shown that, when the HRPY-XAS profiles are extracted naively, the interference results in shifts of the peak positions relative to the conventional XAS resonances and can even produce "false" peaks in completely new positions or erase the correct ones.

We showed that the classic way of producing HRPY-XAS leads to valid results only for a broad class of molecules that have parallel potential energy surfaces of the core-excited and the final state. In order to get lifetime broadening free x-ray-absorption spectra in the general case, we suggest a procedure of removing the lifetime vibrational interference from the 2D map.

ACKNOWLEDGMENTS

We thank Professor M. Simon for the stimulating discussions. This work was supported by the Swedish Research Council (VR), by the STINT Foundation, and by a grant from the Swedish Infrastructure Committee (SNIC) for the project "Multiphysics Modeling of Molecular Materials," No. SNIC 023/07-18. The experiment was carried out with the approval of the JASRI (Proposals No. 2006B1500 and No. 2007A1866) and supported by the Japan Society for Promotion of Science.

[1] J. Stöhr, *NEXAFS Spectroscopy* (Springer, Berlin, 1992).
[2] J. Tulkki and T. Åberg, J. Phys. B **15**, L435 (1982).
[3] W. Drube, A. Lessmann, and G. Materlik, in *Resonant Anomalous X-Ray Scattering. Theory and Applications*, edited by G. Materlik, C. J. Sparks, and K. Fisher (North-Holland, Amsterdam, 1994), p. 473.
[4] P. Eisenberger, P. M. Platzman, and H. Winick, Phys. Rev. Lett. **36**, 623 (1976).
[5] F. Gel'mukhanov and H. Ågren, Phys. Rep. **312**, 87 (1999).
[6] This is not true for dissociative final states: P. Morin and I. Nenner, Phys. Rev. Lett. **56**, 1913 (1986); E. Kukk, H. Aksela, S. Aksela, F. Gel'mukhanov, H. Ågren, and S. Svensson, *ibid.* **76**, 3100 (1996).
[7] K. Hämäläinen, D. P. Siddons, J. B. Hastings, and L. E. Berman, Phys. Rev. Lett. **67**, 2850 (1991).
[8] A. Kivimäki, K. Maier, U. Hergenhahn, M. N. Piancastelli, B. Kempgens, A. Rüdel, and A. M. Bradshaw, Phys. Rev. Lett. **81**, 301 (1998).
[9] F. M. F. de Groot, M. H. Krisch, and J. Vogel, Phys. Rev. B **66**, 195112 (2002).
[10] P. Glatzel, F. M. F. de Groot, O. Manoilova, D. Grandjean, B. M. Weckhuysen, U. Bergmann, and R. Barrea, Phys. Rev. B **72**, 014117 (2005).
[11] Y. Izumi, H. Nagamori, F. Kiyotaki, D. Masih, T. Minato, E. Roisin, J.-P. Candy, H. Tanida, and T. Uruga, Anal. Chem. **77**, 6969 (2005).
[12] H. Hayashi, Anal. Sci. **24**, 15 (2008).
[13] L. Moreschini, C. Dallera, J. J. Joyce, J. L. Sarrao, E. D. Bauer, V. Fritsch, S. Bobev, E. Carpene, S. Huotari, G. Vankó, G. Monaco, P. Lacovig, G. Panaccione, A. Fondacaro, G. Paolicelli, P. Torelli, and M. Grioni, Phys. Rev. B **75**, 035113 (2007).
[14] J.-P. Rueff, L. Journel, P.-E. Petit, and F. Farges, Phys. Rev. B **69**, 235107 (2004).
[15] F. Gel'mukhanov and H. Ågren, Phys. Lett. A **185**, 407 (1994).
[16] Y. Hikosaka, Y. Velkov, E. Shigemasa, T. Kaneyasu, Y. Tamenori, J. Liu, and F. Gel'mukhanov, Phys. Rev. Lett. **101**, 073001 (2008).
[17] F. Kh. Gel'mukhanov, L. N. Mazalov, and A. V. Kondratenko, Chem. Phys. Lett. **46**, 133 (1977).
[18] Y. Velkov, Y. Hikosaka, E. Shigemasa, S. Gavrilyuk, and F. Gelmukhanov, Chem. Phys. Lett. **465**, 153 (2008).
[19] H. Ohashi, E. Ishiguro, Y. Tamenori, H. Okumura, A. Hiraya, H. Yoshida, Y. Senba, K. Okada, N. Saito, I. H. Suzuki, K. Ueda, T. Ibuki, S. Nagaoka, I. Koyano, and T. Ishikawa, Nucl. Instrum. Methods Phys. Res. A **467-468**, 529 (2001).
[20] P. Sałek, Comput. Phys. Commun. **150**, 85 (2003).
[21] T. Tanaka, H. Shindo, C. Makochekanwa, M. Kitajima, H. Tanaka, A. De Fanis, Y. Tamenori, K. Okada, R. Feifel, S. Sorensen, E. Kukk, and K. Ueda, Phys. Rev. A **72**, 022507 (2005).
[22] R. Feifel, A. Baev, F. Gel'mukhanov, H. Ågren, M. N. Piancastelli, M. Andersson, G. Öhrwall, C. Miron, M. Meyer, S. L. Sorensen, A. Naves de Brito, O. Björneholm, L. Karlsson, and S. Svensson, Phys. Rev. A **69**, 022707 (2004).
[23] M. Neeb, J.-E. Rubensson, M. Biermann, and W. Eberhardt, J. Electron Spectrosc. Relat. Phenom. **67**, 261 (1994).
[24] F. Gel'mukhanov, H. Ågren, M. Neeb, J.-E. Rubensson, and A. Bringer, Phys. Lett. A **211**, 101 (1996).
[25] S. Sundin, F. K. Gel'mukhanov, H. Ågren, S. J. Osborne, A. Kikas, O. Björneholm, A. Ausmees, and S. Svensson, Phys. Rev. Lett. **79**, 1451 (1997).
[26] F. Gel'mukhanov, T. Privalov, and H. Ågren, Phys. Rev. A **56**, 256 (1997).
[27] M. Simon, L. Journel, R. Guillemin, W. C. Stolte, I. Minkov, F. Gel'mukhanov, P. Sałek, H. Ågren, S. Carniato, R. Taïeb, A. C. Hudson, and D. W. Lindle, Phys. Rev. A **73**, 020706(R) (2006).
[28] M. Coreno, M. de Simone, K. Prince, R. Richter, M. Vondráček, L. Avaldi, and R. Camilloni, Chem. Phys. Lett. **306**, 269 (1999).
[29] F. Gel'mukhanov and H. Ågren, Phys. Rev. A **54**, 3960 (1996).
[30] C. Såthe, F. F. Guimarães, J.-E. Rubensson, J. Nordgren, A. Agui, J. Guo, U. Ekström, P. Norman, F. Gel'mukhanov, and H. Ågren, Phys. Rev. A **74**, 062512 (2006).
[31] K. P. Huber and G. Herzberg, *Molecular Spectra and Molecular Structure IV* (Van Nostrand Reinhold, New York, 1979).
[32] Y. Song, M. Evans, C. Y. Ng, C.-W. Hsu, and G. K. Jarvis, J. Chem. Phys. **111**, 1905 (1999).